ELSEVIER

International Journal of Minerals, Metallurgy and Materials
Volume 16, Number 6, December 2009, Page 707

Materials

Characterization and wear behavior of WC-0.8Co coating on cast steel rolls by electro-spark deposition

Jian-sheng Wang, Hui-min Meng, Hong-ying Yu, Zi-shuan Fan, and Dong-bai Sun

School of Materials Science and Engineering, University of Science and Technology Beijing, Beijing 100083, China

(Received 2008-11-26)

Abstract: To prepare high wear resistance and high hardness coatings, electro-spark deposition was adopted for depositing an electrode of a mixture of 92wt%WC+8wt%Co on a cast steel roll substrate. The coating was characterized by classical X-ray diffractometer (XRD) and scanning electron microscopy (SEM) with energy dispersive X-ray analysis (EDX). The results indicate that the coating shows nanosized particulate structure and dendritic structure including columnar structure and equiaxed structure. The primary phases of the coating contain Fe_3W_3C, Co_3W_3C, Fe_2C and Si_2W. The coating has a low friction coefficient of 0.13, its average wear-resistance is 3.3 times that of the cast steel roll substrate and the main mechanism is abrasive wear. The maximum microhardness value of the coating is about 1573.9 $Hv_{0.3}$. The study reveals that the electro-spark deposition process has the characteristic of better coating quality and the coating has higher wear resistance and hardness.

Key words: electro-spark deposition (ESD); WC-Co coatings; microstructure; wear resistance

[*This work was financially supported by the International Science and Technology Cooperation Project of the Ministry of Science and Technology of China (No.2006DFA52240).*]

1. Introduction

The electro-spark deposition (ESD) process, in which a pulsed micro-arc between the electrode and the substrate ionizes air to form high-temperature and high-stress areas where alloying occurs, is a surface treatment technology to meet special demands. Due to metallurgical bonding, the coating improves the spalling- and damage-resistance, and the substrate shows no thermal distortion and microstructural change [1-3].

The required equipment, consisting of a pulsed power supply and an electrode holder, is very compact and simple. The electrode holder can be held manually. No process chamber or vacuum system is required. The small physical size allows the production of coatings on large parts and also field service on installed equipment [4].

Within the past years the ESD process has gained increasing interest as a promising technique for the surface treatments of engineering materials due to its efficiency, simplicity and cost-effectiveness [5-8]. For example, it has been successfully used in gas turbine engine components, nuclear reactor components, aeroengine components that would meet rigorous demands to wear, friction, corrosion, and thermal cycling [2, 9-11]. But the ESD process has not been found to be applied on the cast steel roll widely in the metallurgy iron and steel industry.

In the iron and steel industry, the cast steel rolls need high wear-resistance, high corrosion-resistance and high thermal stability. Cemented carbide WC-8Co electrodes are the promising candidates for coatings due to their high hardness, excellent wear and corrosion resistance. Therefore, exploiting a further application of cemented carbide alloys as coatings is of great importance for cast-steel roll in iron and steel plants. In this paper, the preparation of WC-8Co ESD coatings on cast steel rolls, the microstructure, the hardness, the wear-resistant performance and the mechanism of wear resistance were studied. A special emphasis was that the improvements in the coating

Corresponding author: Jian-sheng Wang, **E-mail:** wjs1973425@126.com

Also available online at www.sciencedirect.com

properties were demonstrated by controlling size, shape and distribution of strengthening phases.

2. Experimental

The tungsten carbide coatings were deposited on high carbon cast roll steel coupons by ESD. High carbon cast roll steel (0.68wt% carbon) coupons of 2.54 cm×2.54 cm×1.0 cm were polished using 200, 400, 500, 1000 and 1500 grit emery paper and were subsequently cleaned in alcohol twice prior to deposition. Microstructured electrodes 92wt%WC+8wt%Co was used. The deposition was carried out manually using a hand-held gun at room temperature under argon protection. The power supply was maintained at a voltage of 100 V, a pulse power of 2000 W, and a pulse frequency of 2000 Hz. The electrode rotated at the speed of 2400 r/min.

After deposition, the specimen subsequently were etched by etchants (10vol% KOH+10vol% $K_3[Fe(CN)_6]$+80vol% H_2O). The microstructures of the coating were observed by scanning electron microscopy (SEM) (LEO1450). The phases of the coating were analyzed by Rigaku D/max 2200 pc X-ray. The microhardness was measured on a cross-section surface from the substrate to coating by HVS-1000 digital microhardness tester with a test load of 300 g and a dwelling of 15 s. In the process, 10 microhardness indentations were made at different positions at 5, 15 and 25 μm, respectively, which were the horizontal distance to the sample surface in the coating region. Then the average values of microhardness were calculated at different horizontal distances to the sample surface in the coating region. Using the same processing method, microhardness indentations were made and the mean values of microhardness were measured in the transition zone, heat affected zone and substrate.

A ball-on disc configuration (MM-W1 Tribometer) was employed to investigate the wear behavior of the coated sample. The static partners were the specimens (ϕ 31.7 mm×8 mm) loaded with a normal force of 50 N. Tungsten carbide balls (13 mm in diameter) were against them at a rotary velocity of 200 r/min. The experiments were performed for 15 min at 24ºC and a relative humidity of (50±2)%. Before and after the tests, the specimens were cleaned in acetone solution and then the wear loss was measured using a precision electronic balance (Sartorius BS110) with an accuracy of 1×10^{-4} g.

3. Results and discussion

3.1. Surface morphology of the coating

The sample is characterized by an orange peel appearance as shown in Fig. 1. Thermal expansion mismatch stresses occur between the well-bonded coating and the steel, and then such tensile residual stresses in the ESD coatings lead to the formation of cracks in

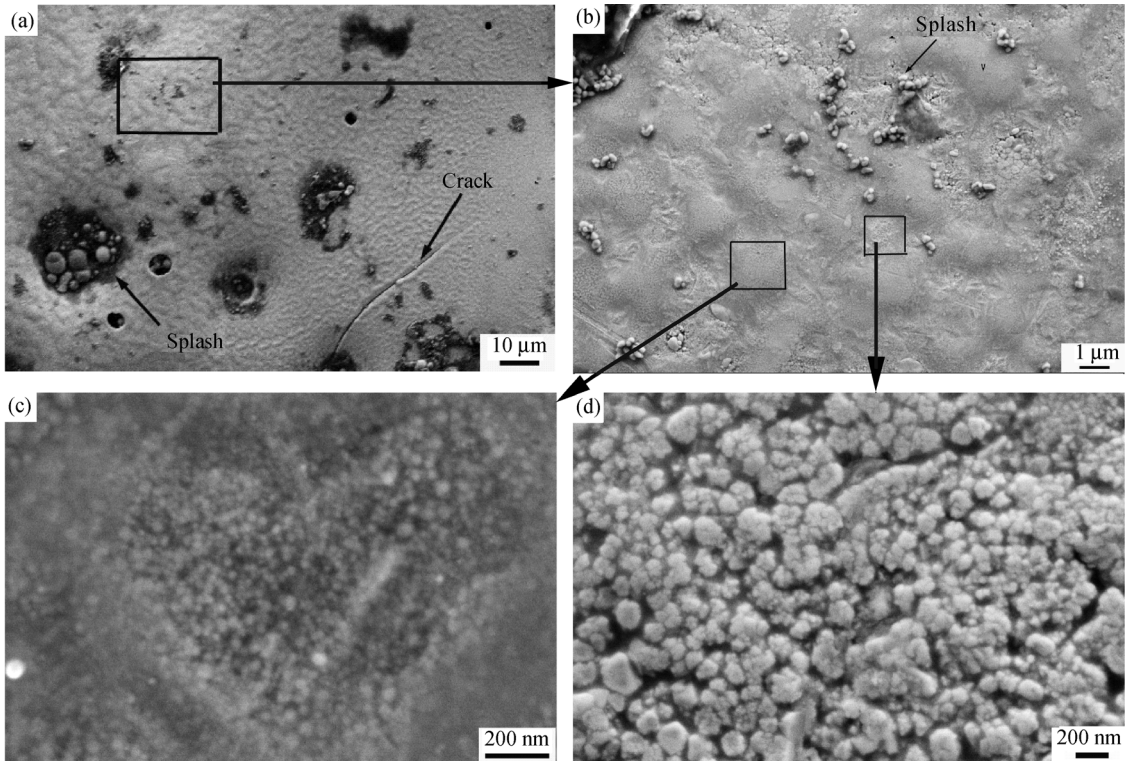

Fig. 1. SEM micrographs of the modified substrate: (a) small region; (b) micro-region with islands; (c) micro-region with nanocrystals; (d) micro-region with cauliflower-like particles.

Fig. 1(a). As indicated by Fig. 1(b), the spatial pattern of the coating tends to exist as islands in the size of about 2 μm. During the ESD process the micro spark between the WC+8Co anode and the substrate leads to molten pools, and then melted metal materials solidify along with the associated shrinkage. As a result, island-shape structures come into as seen in Fig. 1(b). The shape of the coating surface was directly related to deposition parameters during processing, to the degree of washing away of the substrate material and specifically to the morphology of solidified droplets. This morphology is the characteristic of the sample, which has been produced by an ESD process performed in argon atmosphere. It seems that the microstructure is finer inside than that around the islands (Figs. 1(c) and (d)). Islands in Fig. 1(c) show fine nanocrystals while nanocrystals agglomerate into large cauliflower-like particles in Fig. 1(d). These extra-fine structures form on the surface of the sample after depositing.

3.2. Microstructure of the coating

Fig. 2(a) represents the typical cross-section micrographs of the coating. It can be known that ESD produces a dense and strong adherent coating with proper deposition parameters. SEM micrographs of the cross-section of the sample show that the coating is not distributed uniformly. Both the thick coating and thin transition zone are presented in Fig. 2(a). The cross-section micrographs of the coating imply that the temperature gradient during ESD melting is large owing to the employment of a smaller pulse repetition rate. Finer grain sizes of carbide particles have been obtained in these deposition conditions.

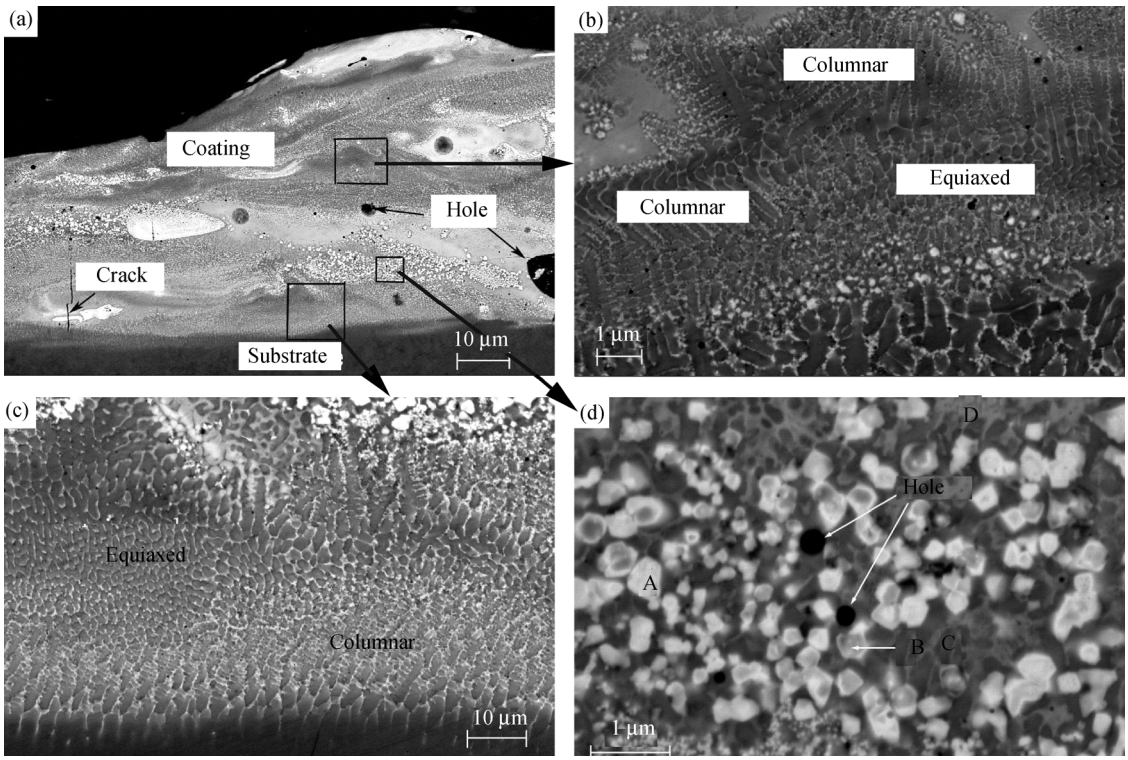

Fig. 2. SEM micrographs (backscattering mode) of the cross-section of the sample: (a) cross-section; (b) the middle of the coating; (c) transition region; (d) white particles region.

The crack observed on the cross-section of the coating (Fig. 2(a)) is perpendicular to the substrate surface due to the fact that the well-bonded coating is placed in tension when it attempts to shrink, while the cooler substrate restricts such shrinkage. Berezhnitskaya [12] has also confirmed the existence of such tensile residual stresses in the ESD coatings.

The microstructures of the coating are composed of fine particulates distributed dispersedly and dendrite structure including columnar structure and equiaxed structure (Figs. 2(b)-(d)), while the microstructures of the transition region tend to change from columnar structure formed in the near zone of the substrate to equiaxed structure formed in the adjacent region of the coating (Fig. 2(c)). They all belong to non-equilibrium structure because of their high cooling rates.

It is well known that the solidification structure of a given alloy is directly influenced by solidification conditions, namely temperature gradient G and solidification rate V. The cooling rate T is defined as the product of G and V. Various solidification morphologies depend on the temperature gradient G and solidification rate V [13]. Generally speaking, the G/V value largely influences morphology growth. During ESD,

the cooling rate may approach 10^5-10^6 K/s and the temperature gradient can reach 10^7-10^8 K/m. When the solidification rate V increases, the temperature gradient G decreases gradually at the same time. As a result, the ratio of G/V decreases gradually and the constitutional supercooling rate becomes large. Thus, the solidification structure will in turn change from planar to cellular, cellular dendrite, columnar dendrite and even equiaxed dendrite, if the fusion pool is large enough and there is enough time for microstructure evolution.

The above microstructural evolution happens at the beginning of solidification of an ESD coating when G is very low, V is very high and the degree of supercooling is next to zero, which results in the limitation of grain growth. As seen in Fig. 2(c), column-like grains grow vertically to the substrate along the build direction. Above the region of column-shape grains is the equiaxed grain region which approaches to the white particulates region. The difference of microstructures between the columnar structure region and the equiaxed structure region can be attributed to the different solidification conditions. As we know, the substrate is cold and the cooling rate approaching to substrate is rather higher than that at the middle stage of the deposited coating. For the growth direction of grains coincides with the heat flux direction, the direction of heat flow is mainly along the deposited layers towards the substrate, the growth of column-like grains is in correspondence with the direction of heat flux. In the region of equiaxed grains, the heat flux direction can not be considered to be unidirectional through the metal and it is also assumed that temperature gradient and solidification velocity are constant along the normal direction of individual melt. Thus the dendrite equiaxed structure forms. In Fig. 2(b), the microstructure is complicated because of the different solidification conditions. The thick deposition layer forms from thin weld deposits layer by layer. The formation of dense layered structure is due to the attribution of metallurgical bonding of ESD process in which a new layer and a previously deposited layer are bonded by such metallurgical reactions as fusion and diffusion. Because countless single-pulse deposition spots randomly overlap each other to make up the thick deposited layer, the surface morphology of the previously deposited layer is uneven. And when a new layer forms, the direction of heat flow is from the new layer to previously deposited layer, which results in columnar structure with different directions (Fig. 2(b)). In someplace of each layer the heat flux is all directional and induces the emergence of equiaxed structure (Fig. 2(b)).

The morphology and microstructures show the coating prevails in nanosized and microsized particulates. During the deposition process, the electrode bumps the steel surface, leading to very high atom diffusion speed. Therefore the phase transformation in the process of electrical discharge heating is diffusion phase transformation. Extra-fine structure results from several factors: the first is the increase of new phase nucleation rate owing to high heating and quick cooling; secondly, new phase nucleation increases due to the increase of dislocations and vacancies with the result of heating and quick cooling. In addition, bumping strain and quick heating equivalence strain is also favorable to grain refinement [14]. The extra-fine structure can greatly improve the wear resistance and hardness of coatings.

3.3. XRD of the coating

Fig. 3 shows the X-ray diffractometer (XRD) of the coating, which indicates that the main phases are Fe_3W_3C, Co_3W_3C, Fe_2C and Si_2W. Energy spectrum analysis is used to analyse the elements at the areas of A, B, C and D in Fig. 2(d). On the basis of the above analysis, the white grain A and the grey grain B in the middle contain Fe_3W_3C or Co_3W_3C which preferably appears from the molten pool as the primary phase during the rapid solidification process. Compound Fe_2C emerges from the dendritic structure of dark area C. Dark area D maybe contains Si_2W. These results indicate that a higher heat input is applied during processing, a higher degree of mixing occurs between the molten substrate and WC+Co from the electrode. This carbide can improve the hardness of the electro-spark deposition coating.

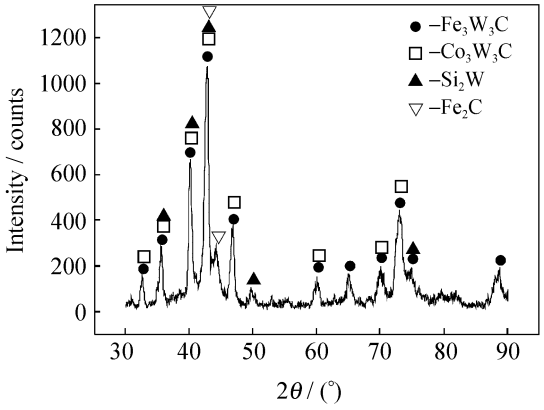

Fig. 3. XRD spectrum of the ESD coating.

3.4. Microhardness of the coating

Fig. 4 shows the microhardness on the sample cross-section. Indentations were carried out in the coating, in the transition region, in the heat affected zone and in the substrate. There were differences between the values of microhardness ($Hv_{0.3}$) at the dif-

ference regions of the samples. The microhardness profile presents graded distribution and rises from the substrate to the upper of the clad coating. The maximum microhardness value of the coating is about $Hv_{0.3}$ 1573.9, which maybe is the point of the carbide. However, a great increase in the average microhardness is observed for the coated samples ($Hv_{0.3}$ 1441±132) compared with the microhardness value of the substrate ($Hv_{0.3}$ 320±10). Another interesting result is related to the microhardness value obtained from measurements carried out in transition zone. This average value of $Hv_{0.3}$ 666.7±112 is nearly two times that of the substrate. High microhardness values of the deposition coating corroborate the findings obtained from the previous micro structural analysis.

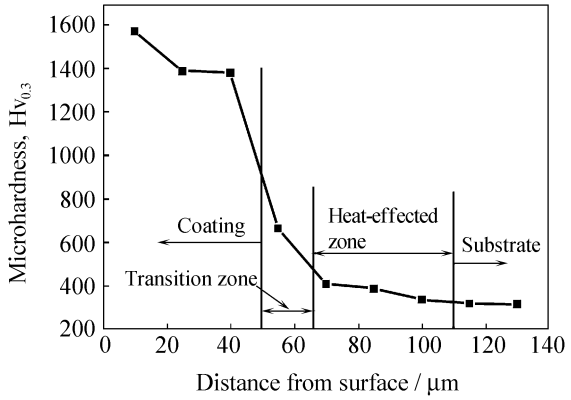

Fig. 4. Microhardness evolution of the deposited coating along the layers.

3.5. Tribological properties of the coating

The wear tests for various tribological samples were carried out. The result shows that the measured values of the mean and maximum friction coefficients of the tested samples do not differ considerably. Fig. 5 shows the representative curves, which describes the evolution of friction coefficient with sliding time for both tribological pairs: deposited sample and tungsten-carbide ball; steel substrate sample and tungsten-carbide ball.

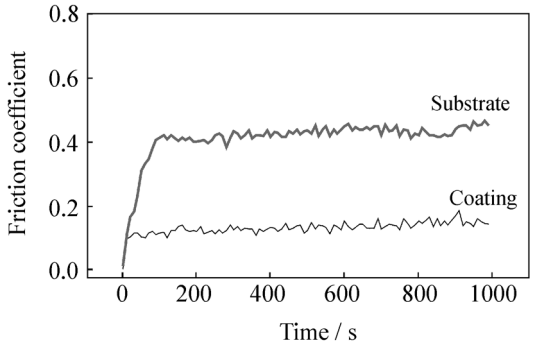

Fig. 5. Evolution of the friction coefficient against sliding time for both tribological pairs: deposited sample and tungsten-carbide ball; steel substrate sample and tungsten-carbide ball.

The abrasive wear results of the coating and high-carbon cast roll steel are listed in Table 1. The wear ratio of the coating is 0.0065 mg/r, and that of the high-carbon steel is 0.0215 mg/r.

The relative wear-resistance ε_w is:

$$\varepsilon_w = \frac{\Delta W_s}{\Delta W_c} = \frac{4.3}{1.3} = 3.31$$

where ΔW_s and ΔW_c are the loss masses of the substrate and coating, respectively.

The wear-resistance of the clad coating is 3.31 times that of the high-carbon steel.

Table 1. Wear test results

Sample	Average friction coefficient	Maximum friction coefficient	Loss mass, ΔW / mg	Wear ratio / ($mg \cdot r^{-1}$)
Coating	0.13	0.19	1.3	0.0065
Substrate	0.43	0.47	4.3	0.0215

The tribological performance of a multiphase coating depends on the characteristics, such as the hardness and thickness of the coating, and the size, distribution and morphology of particles in the coating. As the above mentioned, the coating contains interstitial compounds Fe_3W_3C, Co_3W_3C, Fe_2C and Si_2W which cover the entire substrate. These compounds are significantly more refractory than the pure substrate materials and therefore have high hardness in comparison with the cast steel material. Such microstructural features are elucidated in Fig. 2(b), showing Fe_3W_3C, Co_3W_3C and Fe_2C multiphase particles embedded in the coating. These hard multiphase compounds distributed dispersedly in the coating are the main factors leading to the high hardness and wear resistance of the coating. Moreover, there are many nano- and micro-sized particles in the coating, and their positive effect on tribological characteristics can be explained as follows. According to the Hall-Petch equation, hardness is inversely proportional to the square root of grain size, so the inherent hardness of the coating materials can be improved greatly. In addition to grain refinement, extra fine particles can increase the grain-boundary activity which plays an important role on the load transfer in the strengthening of the coating. It is also possible that nano- and micro-sized particles released on the surface during the wear process are oxidized in the laboratory test environment with a

formation of lubricous oxides.

The wear test belongs to low stress abrasive test, in which the surface material of the part migrates because the abrasives scratch the part's surface under the low stress. In general, abrasive wear resistance is not an intrinsic property of materials but it depends on the tribological system. However, under certain test conditions, the hardness ratio of the abrasive has a great effect on the abrasive wear loss level. When dealing with composite materials, such as tungsten carbide deposition coatings, the hardness ratios of the abrasive and the particulate phase need be considered, respectively. According to Ref. [15], abrasives with equal to or less hardness than that of the worn surface are considered as "soft abrasives". Whereas abrasives harder than the worn surface are regard as "hard abrasives". Particles will be acting as "hard abrasives" against the matrix or as "soft abrasives" against carbides in the coating.

The wear-resistance of the coating is related to the size of particulates, the microstructures and the main phases, which have been discussed above. The coating has good wear-resistance because residual austenite can generate plastic deformation to stop cracks' formation and spreading and also can absorb the work to convert to high-strain martensite, which has high wear-resistance in the wear processing [16-17]. The carbide as a wear resistant has imbedded perfectly in the matrix and is difficult to remove during the wear processing. The wear pattern of the ESD coating is shown in Fig. 6.

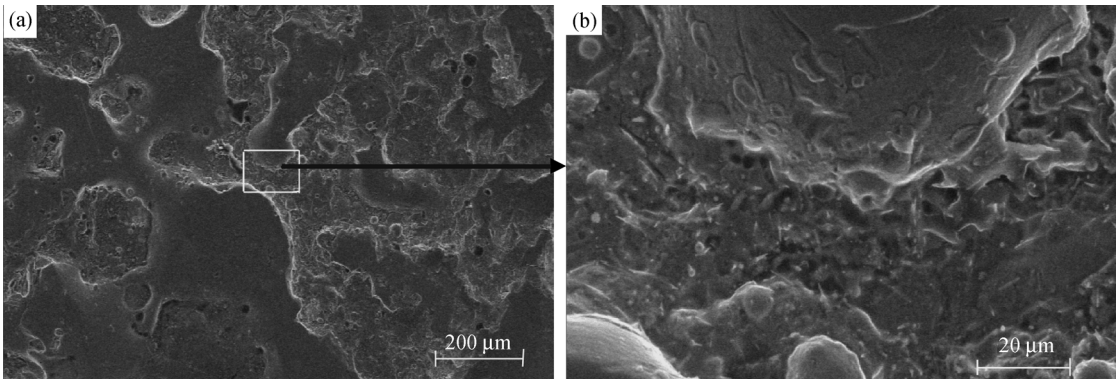

Fig. 6. SEM micrographs of the worn surfaces of a coated steel sample.

In general, the wear mechanisms are mainly adhesive wear, abrasive wear, fatigue wear and oxidation wear under different conditions. There are some relief and debris in Fig. 6. In light of above analysis these debris particulates are carbides. When the hard grains losing from the ball of tungsten carbide pass through the surface of the sample, they meet the carbide, either the hard grains break or the carbide detaches from the coating to form pits and debris. Through the analysis above, it can be known that the main wear mechanism operating on the coating is abrasive wear.

4. Conclusions

(1) The fully dense and strong adherent coating is obtained by ESD. The microstructures of the coating show nanosized particulates and dendritic structure including some columnar and equiaxed structures. The primary phases contain Fe_3W_3C, Co_3W_3C, Fe_2C and Si_2W.

(2) The microhardness presents graded distribution along the depth direction of the coating toward the substrate. The maximum microhardness value of the coating is about $Hv_{0.3}$ 1573.9. The average microhardness value of the coating of the sample is $Hv_{0.3}$ 1441±132. The average microhardness value of the transition zone of the sample is $Hv_{0.3}$ 666.7±112.

(3) The coating has good wear resistance and the average wear resistance rate is 3.3 times that of the cast steel roll substrate. Fine hard phases distributed in the coating dispersedly are the main factors leading the high hardness and wear resistance of the coating. The main wear mechanism is abrasive wear.

References

[1] R.J. Wang, Y.Y. Qian, and J. Liu, Interface behavior study of WC92-Co8 coating produced by electro-spark deposition, *Appl. Surf. Sci*, 240(2005), p.42.

[2] M.H. Staia, A. Fragiel, M. Cruz, E. Carrasquero, B. Campillo, R. Perez, M. Constantino, and T.S. Sudarshan, Characterization and wear behavior of pulsed electrode surfacing coatings, *Wear*, 251(2001), p.1051.

[3] R.N. Johnson, Electro-spark deposition: principles and applications, [in] *Proceedings of the Society of Vacuum Coaters 45th Annual Technical Conference*, Lake BuenaVista, 2002, p.86.

[4] N. Parkansky, R.L. Boxman, and S. Goldsmith, Development and application of pulsed-air-arc deposition, *Surf. Coat. Technol*, 61(1993), p.268.

[5] A. Agarwal and N.B. Dahotre, Pulse electrode deposition of superhard boride coatings on ferrous alloy, *Surf. Coat.*

Technol., 106(1998), p.242.

[6] I.V. Galinov, Investigation of the composition of Ag, Ni and AgNi pseudo-alloy coatings applied by electro-spark alloying on a Cu substrate, *Surf. Coat. Technol.*, 56(1993), p.131.

[7] A.V. Ribalko and O. Sahin, The use of bipolar current pulses in electro spark alloying of metal surfaces, *Surf. Coat. Technol.*, 168(2003), p.129.

[8] N. Parkansky, I.I. Beilis, L. Rapoport, *et al*., Electrode erosion and coating properties in pulsed air arc deposition of WC-based hard alloys, *Surf. Coat. Technol.*, 105(1998), p.130.

[9] R.N. Johnson, Principle and application of electro-spark deposition, [in] *International Conference on Surface Modification Technologies*, Phoenix, 1988, p.188.

[10] R.J. Wang, Y.Y. Qian, and J. Liu, Structural and interfacial analysis of WC92–Co8 coating deposited on titanium alloy by electro-spark deposition, *Appl. Surf. Sci.*, 228(2004), p.405.

[11] S. Frangini, A. Masci, and A. Di Bartolomeo, Cr7C3-based cermet coating deposited on stainless steel by electro-spark process: structural characteristics and corrosion behavior, *Surf. Coat. Technol.*, 149(2002), p.279.

[12] M.F. Berezhnitskaya, A.V. Paustovskii, S.N. Kirilenko, and Y.V. Gubin, Determination of residual stresses in electro-spark deposited coatings, *Strength Mater.*, 35(2003), p.633.

[13] W. Kurz and D.J. Fisher, *Fundamentals of Solidification*, Translation Technology Publications, Switzerland, 1998, p.87.

[14] S.R. Qiao, D. Han, and M. Li, Extra-fine-structure obtained by electrical spark discharge quenching on steel surface, *Mater. Mech. Eng.* (in Chinese), 28(2004), p.7.

[15] S.W. Huang, M. Samandi, and M. Brandt, Abrasive wear performance and microstructure of laser clad WC/Ni layers, *Wear*, 256(2004), p.1095.

[16] A. Yakovlev, Ph. Bertrand, and I. Smurov, Laser cladding of wear resistant metal matrix composite coatings, *Thin Solid Films*, 453(2004), p.133.

[17] Q.L. Wu, Y.S. Sun, and G.Q. Li, Microstructure and wear properties of the electroslag remelting layer reinforced by TiC particles, *J.Univ. Sci. Technol. Beijing*, 15(2008), p.769.